

## RESEARCH LETTER

10.1002/2016GL072417

## Key Points:

- Tohoku earthquake triggers seismicity approximately 9800 km away
- Local earthquakes triggered by Rayleigh waves
- Simulations of passing seismic waves across a high-resolution velocity map of a well-studied geothermal field

## Supporting Information:

- Figure S1

## Correspondence to:

M. Lupi,  
matteo.lupi@unige.ch

## Citation:

Lupi, M., F. Fuchs, and E. H. Saenger (2017), Numerical simulations of passing seismic waves at the Larderello-Travale Geothermal Field, Italy, *Geophys. Res. Lett.*, *44*, doi:10.1002/2016GL072417.

Received 17 JUN 2016

Accepted 1 MAY 2017

Accepted article online 3 MAY 2017

## Numerical simulations of passing seismic waves at the Larderello-Travale Geothermal Field, Italy

Matteo Lupi<sup>1</sup> , Florian Fuchs<sup>2</sup> , and Erik H. Saenger<sup>3,4</sup>

<sup>1</sup>Department of Earth Sciences, University of Geneva, Geneva, Switzerland, <sup>2</sup>Department of Meteorology and Geophysics, University of Vienna, Vienna, Austria, <sup>3</sup>International Geothermal Centre, Hochschule Bochum, Germany, <sup>4</sup>Ruhr-Universität Bochum, Bochum, Germany

**Abstract** Passing seismic waves released by large-magnitude earthquakes may affect geological systems located thousands of miles far from the epicenter. The  $M_{9.0}$  Tohoku earthquake struck on 11 March 2011 in Japan. We detected local seismic activity at the Larderello-Travale geothermal field, Italy, coinciding with the maximum amplitudes of the Rayleigh waves generated by the Tohoku earthquake. We suggest that the earthquakes were triggered by passing Rayleigh waves that induced locally a maximum vertical displacement of approximately 7.5 mm (for waves with period of 100 s). The estimated dynamic stress was about 8 kPa for a measured peak ground velocity of 0.8 mm/s. Previous similar observations pointed out local seismicity at the Larderello-Travale Geothermal Field triggered by the 2012  $M_w$  5.9 Po Plain earthquake. We conducted forward numerical modeling to investigate the effects caused by passing  $P$ ,  $S$ , Love, and Rayleigh waves through the known velocity structure of the geothermal field. Results indicate that maximum displacements focus differently when considering body or surface waves, with displacement values being higher within the first 2 km of depth. The focusing of the displacement below 3 km seems to be strongly controlled by the velocity structure of the Larderello-Travale geothermal field. We propose that seismic activity triggered by passing seismic waves may be related to a clock-advancing mechanism for local seismic events that may have occurred in any case. Furthermore, our analysis shows that local anisotropies in the velocity structure of the Larderello-Travale geothermal field (possibly linked to compartments of elevated pore pressures) strongly control the reactivation of regions of the geothermal field affected by passing seismic waves.

### 1. Introduction

Earthquakes impose static and dynamic stresses that may be sufficient to reactivate quiescent geological systems [e.g., Hill *et al.*, 2002; Freed, 2005; Steacy, 2005; Manga and Brodsky, 2006]. Static and dynamic stress triggering involve different geological and geophysical processes. While static stress triggering is due to the change of the shear and normal stress acting on geological systems near to the earthquake rupture zone [Stein, 1999], dynamic stresses act during the passage of the seismic waves released by the earthquake [e.g., Hill *et al.*, 2002; Manga and Brodsky, 2006]. Static stress triggering reaches maximum distances on the order of the length of the ruptured fault zone, while dynamic stress triggering can reach the far field (i.e., thousands of kilometers). Pioneering studies highlighting dynamic triggering were associated to the 1993  $M7.4$  Landers, California [Hill *et al.*, 1993], and 2002  $M7.9$  Denali, Alaska [Gomberg *et al.*, 2001], earthquakes. For instance, Prejean [2004] shows that following the 2002  $M7.9$  Denali earthquake, intense seismicity was triggered along the North American Pacific coast. Husen *et al.* [2004] highlight that geysers at the Yellowstone Park, U.S., changed their eruptive behavior. Additionally, Gomberg *et al.* [2004] and Husen *et al.* [2004] point out how nucleation of local seismic events often coincides with the passage of the seismic waves.

Today dynamic triggering is often discovered in geological systems in a near-critical state (i.e., characterized by elevated pore pressures at depth or critically stressed [e.g., Jousset and Rohmer, 2012]). Megathrust earthquakes produce large amounts of seismic energy and frequently trigger geological responses in the far field [Miyazawa and Mori, 2006; Walter and Amelung, 2007; Peng *et al.*, 2010; Kiser and Ishii, 2011; Fry *et al.*, 2011; Ryder *et al.*, 2012; Gonzalez-Huizar *et al.*, 2012; Zigone *et al.*, 2012; Pollitz and Bürgmann, 2014].

Gonzalez-Huizar *et al.* [2012] show that the M9.0 Tohoku earthquake triggered both tremor and local earthquakes across various places worldwide. Prejean [2013] suggests that geothermal systems are more sensitive than magmatic systems to incoming seismic energy and triggered responses should be more common in such geological environments. Saccorotti *et al.* [2013] highlight that the Larderello-Travale geothermal field (LTGF) is sensitive to displacements caused by passing seismic waves as local seismicity (normally occurring between 4 km and 9 km depth [Vanorio *et al.*, 2004; De Matteis *et al.*, 2008]) was enhanced by the 2002 M5.9 Po Plain earthquake sequence [Piccinini *et al.*, 2012]. Similar findings were suggested for the Lusi sedimentary-hosted hydrothermal system where body waves triggered the release of fluids from depth [Lupi *et al.*, 2013, 2014]. In this manuscript we point out that the seismic activity of the LTGF may have been affected by the passing waves released by the M9.0 Tohoku earthquake that occurred in Japan in 2011. We locate the triggered events and estimate the maximum dynamic stress imposed by passing seismic waves. Next, we run forward simulations of passing  $P$ ,  $S$ , Love, and Rayleigh waves across the measured velocity structure of the LTGF [Vanorio *et al.*, 2004; De Matteis *et al.*, 2008]. This allowed us to quantify the displacement caused by passing seismic waves at various depths at the LTGF and understand how dynamic triggering may operate in this geothermal field. Our findings are then discussed and compared to previous studies before drawing the main conclusions.

## 2. The Larderello-Travale Geothermal Field

The LTGF is located in Central Tuscany, Italy. The LTGF is part of the Tuscan Magmatic Province emplaced since the early Miocene during the slab rollback in the collision of the Sardinia-Corsica and the Adria plates [Malinverno and Ryan, 1986; Keller and Pialli, 1990; Dini *et al.*, 2005]. The LTGF is marked by extensional tectonics that began in the Pliocene [Brogi, 2005]. The normal faults are associated with the latest Pliocene extensional episode [Malinverno and Ryan, 1986; Keller and Pialli, 1990; Dini *et al.*, 2005]. At approximately 3 km depth the LTGF is characterized by a horizon (more precisely a marked seismic reflector) known as the k horizon. The k horizon is suggested to be characterized by the presence of supercritical fluids hosted in fractured lithologies [Bertini *et al.*, 2006], and it is thought to represent the brittle-ductile boundary. Vanorio *et al.* [2004], De Matteis *et al.* [2008], and Saccorotti *et al.* [2014] propose high-resolution  $V_p$  and  $V_s$  wave velocity maps for the LTGF pointing out regions characterized by the presence of liquid and vapor phases at depth. We used such velocity maps to build our model.

The LTGF is marked by regions of reduced  $V_p/V_s$  anomalies due to very low  $V_p$  velocities (i.e., interpreted as geological compartments characterized by the presence of a vapor phase [De Matteis *et al.*, 2008]). Vice versa, regions of high  $V_p/V_s$  ratios, due to elevated  $V_p$  values, occur at shallow depths and have been interpreted by De Matteis *et al.* [2008] as reflecting the presence of liquid phases (i.e., downwelling of groundwater or condensation zones). The average heat flow of the area is about 120 mW/m<sup>-2</sup> with maximum values as high as 1000 mW/m<sup>-2</sup> [Baldi *et al.*, 1995]. This implies temperatures as high as 250°C at 1 km depth.

## 3. Data

### 3.1. Triggered Local Earthquakes

Previous studies showed that the LTGF is sensitive to regional earthquakes [Saccorotti *et al.*, 2013]. After a preliminary inspection of the seismic data recorded at the LTGF we noticed that the M9.0 Tohoku earthquake in 2011 (approximately 9800 km away) may have triggered seismic activity at the LTGF. To verify this observation, we used publicly available data from seismic stations of the Italian broadband seismic network [Mele *et al.*, 2007] operated by the Istituto Nazionale di Geofisica e Vulcanologia (INGV) to locate and investigate the seismic events. Eleven permanent seismic broadband stations (with sampling rates >80 sps) were installed within 80 km around the LTGF during March 2011. For nine of these, high sampling rate waveform data are available at the European Integrated Data Archive (EIDA). We retrieved the waveform data and metadata for the seismic stations ARCI, CASP, CSNT, FROS, LATE, MCIV, SACS, SASS, and TRIF. All stations have identical instrumentation (three-component Nanometrics Trillium 40, except SACS which is equipped with a Trillium 120) and provide ground velocity data at 125 sps (FROS, SASS, TRIF, and MCIV) or 100 sps (ARCI, CASP, CSNT, LATE, and SACS). In Figure 2a the top three traces show the rotated (vertical, radial, and transverse) and unfiltered velocity waveforms of the Tohoku earthquake as recorded on station FROS, which is situated at the eastern edge of the LTGF. To determine the maximum ground displacement and maximum ground velocity induced by the surface waves generated by the Tohoku earthquake at the LTGF, we calculate instrument-corrected seismograms (both in units of displacement and velocity) and read the maximum amplitudes of Rayleigh and Love waves.

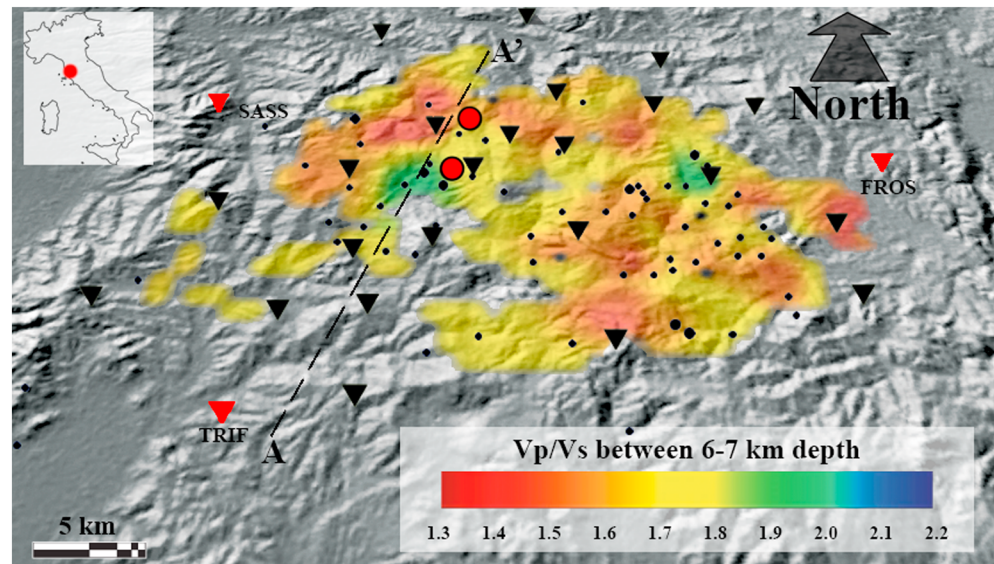


**Figure 1.** Map of LTGF with  $V_p/V_s$  ratio distribution between 6 km and 7 km depth (map adapted from *De Matteis et al.* [2008]). The black dots are taken from the INGV catalog and indicate the local seismic activity 6 months before and 6 months after 11 March 2011. The dashed black line shows the position of the cross section used for the numerical simulation shown in Figures 3 and 4. The inverted triangles point out the location of the seismic stations used by *De Matteis et al.* [2008] to invert for the velocity model. The red inverted triangles show the location of the seismic stations used to locate the seismic events triggered by the passing seismic waves generated by the M9.0 Tohoku earthquake. For geographical reference the stations FROS, TRIF, and SASS have coordinates of 43.20972 and 11.15622, 43.11478 and 10.90265, and 43.06298 and 12.65175, respectively. ARCI, CASP, and CSNT seismic stations are not on the map as they are too far and their coordinates are in latitude-longitude 42.85, 11.48; 42.79, 10.87; and 43.47, 11.29, respectively. The velocity model used to locate the local events is the following: depth,  $V_p$ ,  $V_s/0$ , 4.68, 2.54/ 0.5, 4.68, 2.59/ 1, 4.68, 2.63/ 1.5, 4.68, 2.71/ 2, 4.68, 2.82/ 2.5, 4.81, 3.00/ 3, 4.98, 3.07/ 3.5, 5.17, 3.11/ 4, 5.20, 3.11/ 4.5, 5.26, 3.11/ 5, 5.36, 3.11/ 5.5, 5.41, 3.11/ 6, 5.50, 3.11/ 6.5, 5.64, 3.11/ 7, 5.67, 3.11/ 7.5, 5.74, 3.17/ 8, 5.75, 3.17/ 8.5, 5.77, 3.17/ 9, 5.80, 3.17/ 15, 7.92, 3.17.

The maximum vertical ground displacement caused by Rayleigh waves at the LTGF is approximately 7.5 mm (averaged over the three stations near the geothermal field: FROS, SASS, and TRIF) and is reached during the first arriving Rayleigh waves that have a period of approximately 100 s. Later in the coda, we measure a vertical ground displacement of 1.5 mm from Rayleigh waves with a period of 20 s (simulated in this work, see below for discussion about the selected period). The first arrival of the Love waves (central period of 185 s) cause an average horizontal displacement of 8 mm, while coda Love waves of 20 s period (simulated in this work) induce 1.8 mm of horizontal displacement. The dynamic stresses ( $\sigma_D \sim \mu \cdot PGV \cdot v_s^{-1}$ ) associated with the passage of the Rayleigh waves are approximately 8 kPa (estimated from the peak ground velocity 0.8 mm/s, 30 GPa shear modulus, and  $V_s = 3$  km/s [*De Matteis et al.*, 2008]). Note that we read ground displacement rather than the common ground velocity in order to calibrate the numerical simulations. We did not compare our amplitude reading to theoretical amplitudes since we rely on the correctness of INGV metadata. We read amplitudes for very long period surface waves (up to 100 s) which is beyond the flat part of the transfer function of the Trillium 40.

To reveal potential local seismic activity at the LTGF, we applied a 5–15 Hz bandpass filter to the data recorded during the Tohoku earthquake, which effectively removes the low-frequency signal generated by the megathrust earthquake. The filtered waveforms (Figure 2b) show the occurrence of two local earthquakes during the passage of the surface waves generated by the Tohoku earthquake (red dots in Figures 1, 3, and 4). Clear signals of the local earthquakes can be identified only at stations FROS, SASS, and TRIF (Figure 1) and ARCI, CASP, and CSNT (outside the area of Figure 1). We locate both earthquakes inside the LTGF (Figure 1) with lateral uncertainties of  $\pm 2$  km. We obtain depths of 6.3 km and 8.6 km, respectively, as best fitting results. However, depth is only loosely constrained with errors of approximately 3 km depth. For locating the potentially triggered events we used the Hypocenter code [*Lienert and Havskov*, 1995] and a 1-D velocity model (with layer thickness of 500 m) based on the  $V_p$  and  $V_s$  velocities of *De Matteis et al.* [2008] (the velocity model is reported in the caption of Figure 2). For the calculation of the local magnitude we use the procedure and distance

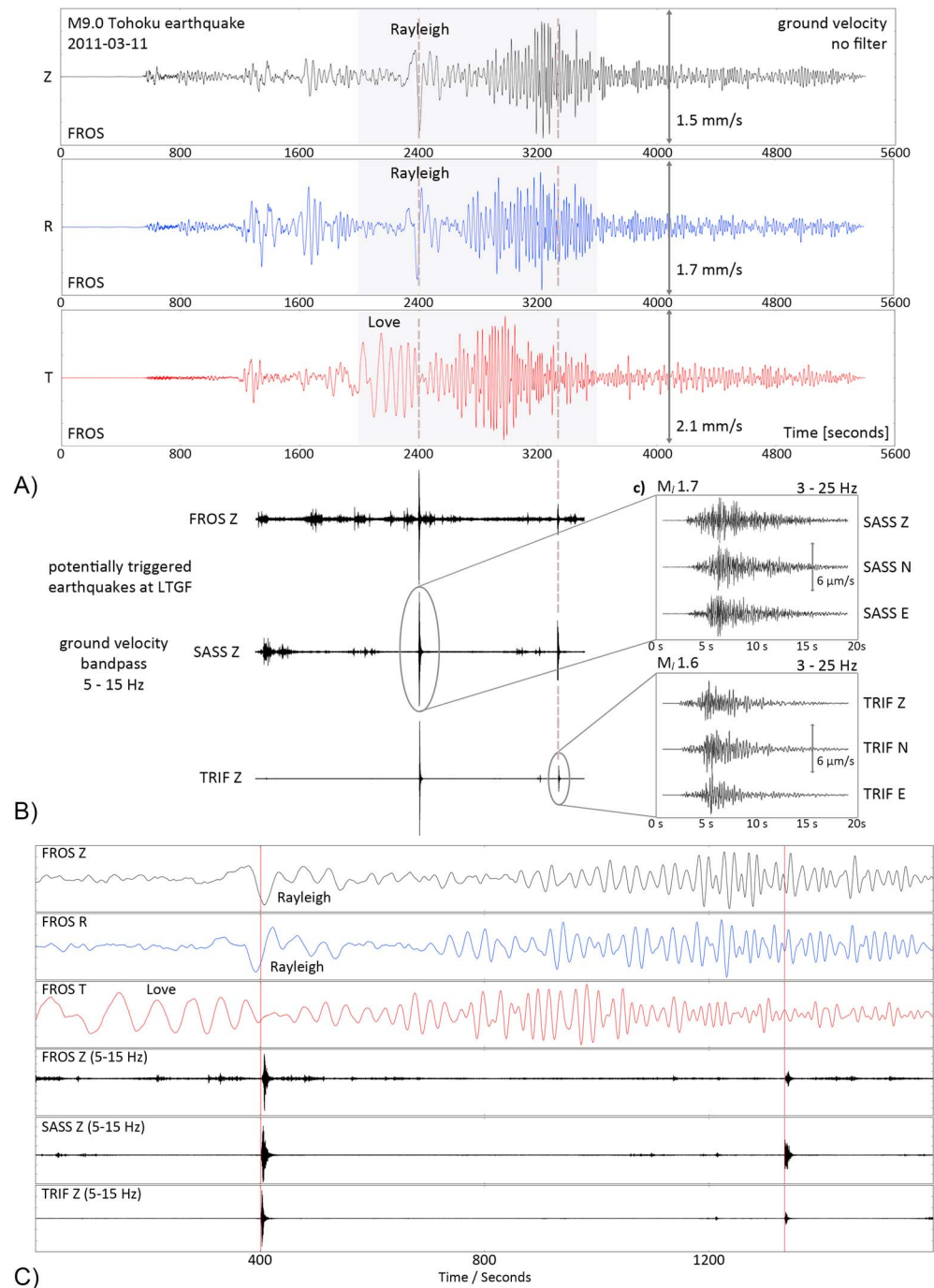


**Figure 2.** Triggered earthquakes at Larderello-Travale geothermal field. (a) The upper three traces show unfiltered ground velocity (raw data, not instrument corrected) on the vertical (Z), radial (R), and transverse (T) components of the 2011  $M_{9.0}$  Tohoku earthquake measured on station FROS. Vertical arrows mark the amplitude scale read from response corrected data. Dashed vertical lines mark the first arrivals of Rayleigh waves (Z and R) and Love waves (T). (b) The three traces show velocity waveforms from stations FROS, SASS, and TRIF (vertical component only). To reveal the local earthquakes over the background Tohoku signals, we applied a 5–15 Hz bandpass filter. Time scale is identical to panel above. (c) Zoom in on the two triggered events as recorded on SASS and TRIF, respectively, with a bandpass filter of 3–25 Hz for best visibility. The red lines show the timing of the two possibly triggered earthquakes.

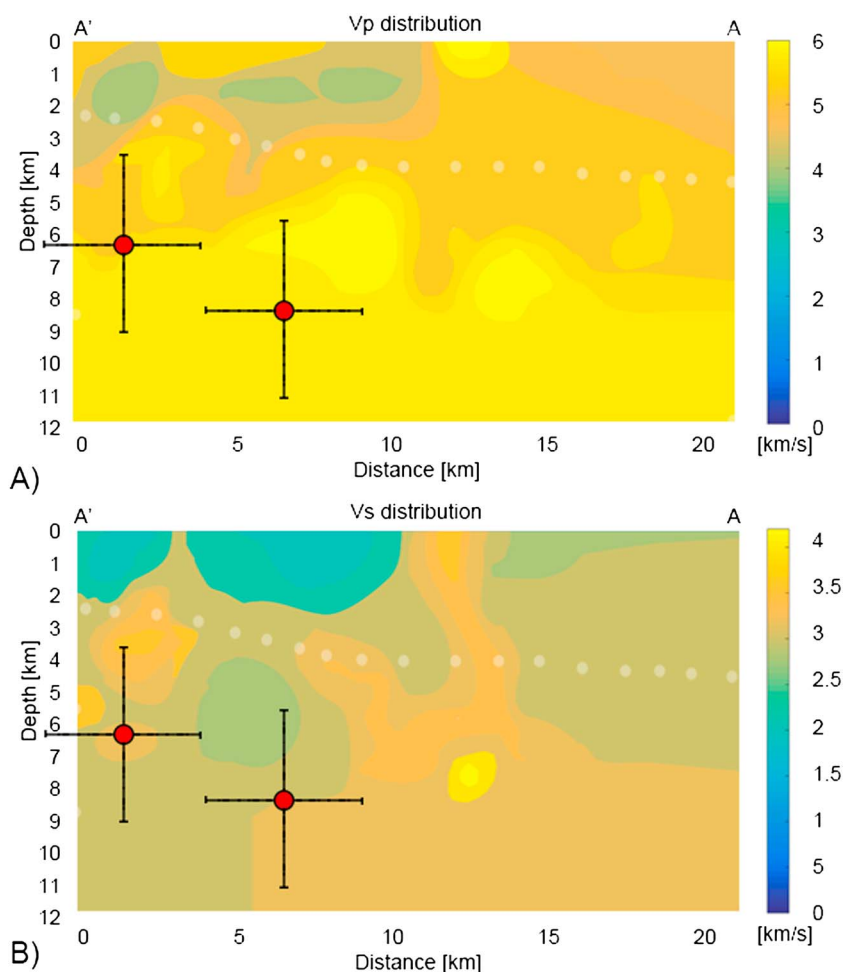


**Figure 3.** Geometry and velocity structure of the Larderello-Travale geothermal field. (a)  $V_p$  and (b)  $V_s$  distribution. The direction of the cut A-A' is shown in Figure 1. The red circles show the location of the local earthquakes possibly triggered by the  $M_{9.0}$  Tohoku earthquake, and the black bars indicate the uncertainty of our localizations. The brittle-ductile transition, i.e., the k horizon [Brogi *et al.*, 2003], is thought to occur at around 4 km depth and is marked by the white dotted line.

corrections as introduced by Hutton and Boore [1987], which is identical to the one used for the local magnitudes in the INGV catalog [Lolli *et al.*, 2015]. The first local earthquake of magnitude  $M_l$  1.7 coincides with the arrival of the first Rayleigh waves (period of 100 s) that induce the maximum vertical displacement at the surface of 7.5 mm. At the time of this earthquake there is no significant ground motion from Love waves. On the recordings of station FROS the arrival of the Pg phase of the triggered earthquake is registered approximately 7 s after the maximum negative velocity of the very first cycle of the Rayleigh waves. A surface wave front recorded at FROS arrives at the triggered earthquake source volume approximately 3 s later (given the 12 km along-great-circle-path difference and assuming 3.8 km/s Rayleigh phase velocity). From the hypocenter, the P wave of the triggered earthquake takes approximately 4–5 s to be recorded at FROS (24 km direct line-of-sight distance, average P wave velocity of 5.1 km/s; see Figure 3). This may explain the observed delay of approximately 7 s. We suggest that the first local earthquake was triggered during the very first downward motion of the Rayleigh wave generated by the Tohoku earthquake. The second local earthquake of magnitude  $M_l$  1.6 occurs approximately 15 min later during the surface wave coda. At this stage the teleseismic wave field is dominated by Rayleigh and Love waves of around 20 s period and 1.5 mm displacement.

### 3.2. Numerical Simulations of Passing Seismic Waves

Saccorotti *et al.* [2013] first showed that the LTGF is sensitive to incoming seismic energy and pointed out that seismic waves generated by the 2012 Po Plain seismic sequence [Piccinini *et al.*, 2012] triggered local seismic activity at the LTGF. To investigate how passing body and surface waves may trigger local seismicity at the

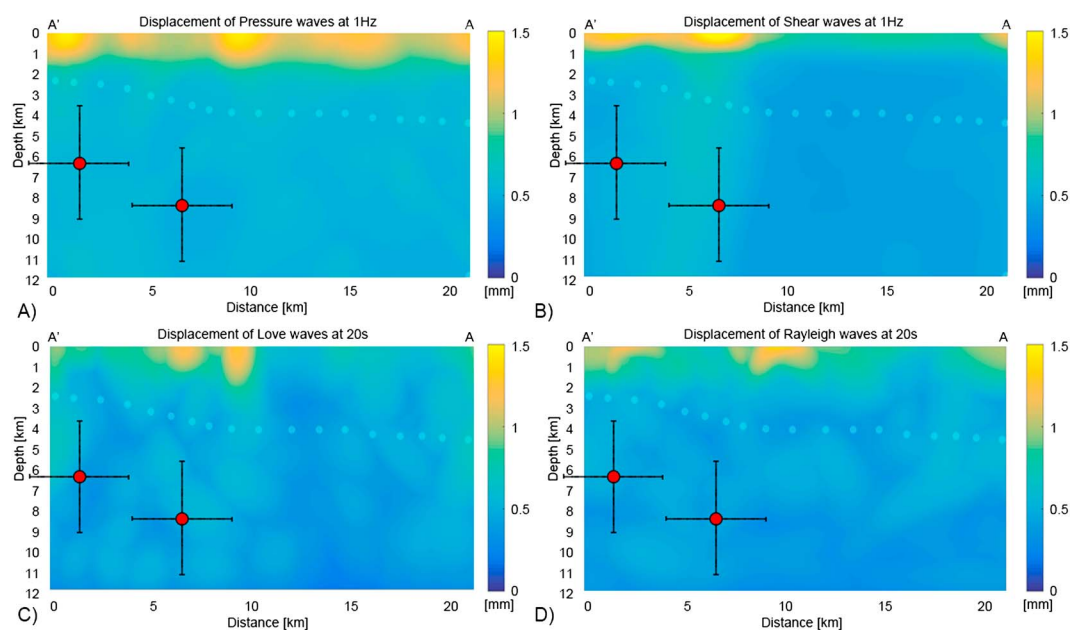


**Figure 4.** Results of the numerical study. Maximum displacement induced by passing (a)  $P$  waves, (b)  $S$  waves, (c) Love waves, and (d) Rayleigh waves. The dotted line indicates the  $k$  horizon that is suggested to represent the brittle-ductile transition.

LTGF, we simulated synthetic body waves with central frequency of 1 Hz and surface waves with central period of 20 s using the method described in *Saenger et al.* [2000]. We calibrate our results for body and surface waves by imposing at the surface the same displacement generated by body and surface waves recorded at seismic stations at the LTGF. While the displacement induced by the 2012 Po Plain seismic sequence at LTGF varies from 1 mm to approximately 2 mm (depending on the shock considered from the Po Plain seismic sequence) and was mainly due to higher frequency body waves, the maximum displacement from the  $M9.0$  Tohoku earthquake imposed on the LTGF was due to surface waves with a period of  $\sim 100$  s. However, we could not simulate such long periods for hardware limitations as it would have required a too large model (i.e., a 10 times longer period requires a 100 times larger model). We selected Love and Rayleigh waves with periods of 20 s because wave trains with central period of 20 s have been shown to be particularly effective in pumping upward deep fluids from the lower crust [*Hill, 2012*]. Additionally, *Saccorotti et al.* [2013] point out that waves with central periods around 10 s caused triggered seismic activity at the LTGF. Using the central period of 20 s still provides a clear picture of the regions of the geothermal field that may be affected by higher accumulations of seismic energy density. Additionally, our forward modeling only accounts for a monofrequency wave passing through the system while earthquakes release waves with different frequencies and periods affecting simultaneously a given geological system. This implies that our work shows a conservative quantification of the effective displacement imposed by passing seismic waves. It follows that our findings represent the lowest limit of the stresses imposed on the LTGF by passing seismic waves, and the cumulative dynamic stress may therefore have been higher.

The velocity model for our simulations (Figure 3) is reconstructed from the velocity structure ( $V_p$  and  $V_s$ ) of the LTGF [*Vanorio et al., 2004; De Matteis et al., 2008; Saccorotti et al., 2014*], and densities are assumed constant at  $1850 \text{ kg/m}^3$ . This is an assumption as the LTGF may be characterized by sharp density contrasts due to the presence of superheated fluids, brines, and different geological units. We run sensitivity tests varying the density of the model with densities ranging from  $1500 \text{ kg/m}^3$  to  $2800 \text{ kg/m}^3$ . Results show the same order of magnitude of displacement (Figure 4), despite the density value chosen. It should be pointed out that *Della Vedova et al.* [2008] provide temperature and gravity anomalies for the LTGF that may be linked to density variations at depth. However, such information is much coarser when compared to the velocity model that we use. Hence, we have no constraints on possible sharp variations due to vapor-saturated reservoirs or to dry units. Our approximation on the density does not represent the complex density heterogeneity of the LTGF, but it prevents us from introducing any arbitrary contrast of impedance and makes us rely on measured values only [i.e., *Vanorio et al., 2004; De Matteis et al., 2008*]. Our impedance contrasts are only related to changes in

measured seismic wave velocities occurring at depth. The detailed two-dimensional model measures 22 km and reaches 9 km depth. We discretized the model into a rotated staggered finite difference grid [Saenger *et al.*, 2000] of  $1801 \times 4601$  nodes with a grid spacing of 5 m. We applied periodic boundary conditions at the left and right boundaries. The top boundary is a free surface, and at the bottom we applied absorbing boundary conditions. The amplitude of the incoming wave is constrained such that the average horizontal displacement at the surface in the simulations is fixed at 1.5 mm. Body waves are generated as planar waves entering the model from the bottom boundary, while surface waves are introduced from the top right corner of the model.

#### 4. Discussion and Conclusions

The two earthquakes that we report are not listed in the seismic catalog of INGV that is complete for magnitudes  $M_l > 1.6$  in the area of the LTGF [Mele *et al.*, 2007; Saccorotti *et al.*, 2013]. However, the magnitudes that we determine are near the detection limit of the INGV network and they may have evaded automatic detection because their signals were obscured by the seismic waves generated by the Tohoku earthquake. Although we cannot entirely rule out that the two earthquakes occurred as regular seismic activity in the LTGF and accidentally coincided with Rayleigh waves, we investigated whether both earthquakes could have been dynamically triggered by the passage of the seismic waves. From 2009 to 2013 the INGV catalog lists on average 0.2 earthquakes with  $M_l > 1.0$  per day in the greater Larderello-Travale area. De Matteis *et al.* [2008] report 500 microearthquakes of  $M_l$  between 0.0 and 3.0 from 1994 to 2000 recorded by a dense local station network, similarly resulting in an average 0.2 earthquakes per day. To compare the potentially triggered seismicity to the natural seismicity, we compiled a list of all earthquakes recorded by the INGV network with  $M_l > 0.0$  and within a 20 km radius around the epicenter of the triggered candidates (which covers the extension of the LTGF) in the 6 months before and 6 months after the Tohoku earthquake (Figure S1a). Within the 30 days prior to the Tohoku earthquake two earthquakes of magnitudes  $M_l$  1.5 and  $M_l$  2.1 occurred at 10 km and 18 km depth, southeast of the two events shown in Figure 1. Within the 30 days after the Tohoku earthquake only a single  $M_l$  1.7 event is registered 25 km southwest of the red epicenters in Figure 1. The period from mid-February 2011 to May 2011 is seismically quiet (Figure S1a). Additionally, subsequent earthquakes with interevent time of less than a day are only observed during swarm periods (e.g., January, July, or August 2011). This is not the case for March 2011.

We also conducted a manual inspection for local earthquakes with magnitude lower than the completeness magnitude for the LTGF to ensure not to underestimate the natural seismicity. We scanned waveform data of the three stations closest to the LTGF (FROS, SASS, and TRIF) for a time span covering 2 months before and 1 month after the Tohoku earthquake using an STA/LTA trigger. With 5 s and 20 s window lengths for STA and LTA, respectively. We required successful detection (STA/LTA threshold = 4) on all three stations on vertical component data bandpass filtered from 5 to 20 Hz. With this setting we were able to find all events listed in the INGV catalog and the two potentially triggered earthquakes with almost no false alarms. Additionally, within the 3 month time frame we found additional 36 local earthquakes within the LTGF with  $M_l < 1.6$  not listed in the INGV catalog (see Figure S1a).

To further verify the likelihood of dynamic triggering on 11 March at LTGF, we calculated the  $\beta$  value [Matthews and Reasenberg, 1988; Aron and Hardebeck, 2009], which compares the number of events during a potential triggering window with the number of events before the triggering window [Matthews and Reasenberg, 1988; Aron and Hardebeck, 2009]. A  $\beta$  value  $> 2$  is an indicator for a statistically significant increase of seismicity during the triggering window. Our triggering window length is 30 min (corresponding to the duration of surface wave shaking at LTGF) including two potentially triggered events. The resulting beta value ranges from 9.8 (no additional pretriggering events within 1 day preevent time) through 15.4 (two additional pretriggering events within 5 days preevent time) up to  $> 19$  (15 additional pretriggering events within 34 days preevent time). Figure S1b shows the  $\beta$  value for different preevent time windows. Although the robustness of the results of the  $\beta$  value is limited in our case by the small number of total events [Hill and Prejean, 2015], the generally high  $\beta$  values support the observation that the two local events may be dynamically triggered. Hence, we speculate that the two detected earthquakes of  $M_l$  1.7 and  $M_l$  1.6 occurring precisely during the maximum amplitudes of the arrival of the Rayleigh waves generated by the Tohoku earthquake might not have been a random occurrence.

Figure 4 shows the distribution of the displacement for  $P$ ,  $S$ , Love, and Rayleigh waves traveling through the LTGF pointing out that body and surface waves affect the system differently.  $P$  and  $S$  waves generate overall larger displacements within 1 km depth (Figures 4a and 4b). Surface waves cause displacements at the surface confined to specific regions marked by strong velocity contrasts (Figure 3). Medium displacements (i.e., about half of the maximum values recorded at the surface) occur beneath the  $k$  horizon. Compared to body waves, surface waves impose a more patchy distribution of medium displacement (Figures 4c and 4d). The large error on the location of the triggered events only allow us to speculate about the possible correlation between the hypocenter of the triggered earthquakes and regions marked larger displacements. However, it must be noticed that the deeper triggered event (i.e., the earthquake with hypocenter at 8.6 km depth) seems to fall in a compartment affected by larger dynamic displacements (Figures 4b and 4c). *Saccorotti et al.* [2013] point out that the seismic events triggered at the LTGF by the passage of Rayleigh waves released by the 2012 Po Plain seismic sequence occurred at 4 km and 6 km depth. Our numerical simulations indicate that sharp variations in the velocity structure of the LTGF are key to explain focusing of seismic energy and, hence, displacement. While we acknowledge that *Saccorotti et al.* [2013] find that local triggered seismic activity coincided with the passage of Rayleigh waves, our simulations also indicate that body (and in particular shear) waves may have relevant effects at depth. At short epicentral distance, i.e., less than 250 km from the epicenter, the seismic displacement is mainly caused by body waves [*Kulhánek*, 2002]. The 2012 Po Plain seismic sequence occurred less than 200 km away from the LTGF implying that body waves may have also contributed in imposing dynamic stress at the LTGF. Based on our numerical results, we speculate that for the Po Plain case presented by *Saccorotti et al.* [2013], the arrival of shear waves may have affected the already critically stressed fault systems of the LTGF. Next, as also suggested by *Saccorotti et al.* [2013], the arrival of the Rayleigh waves imposed the necessary stress to rupture the faults already close to failure due to the presence of pore fluids at near-lithostatic or supralithostatic pressure. This mechanism is in agreement with the findings of *Saccorotti et al.* [2013] and develops from the observations of *Hill* [2012] who point out how surface waves may be particularly effective in mobilizing deep geothermal and magmatic fluids resulting in crack opening, i.e., local seismic activity.

Possibly, the largest discrepancy of our work is related to the occurrence of triggered seismic activity at depth, rather than in the shallow region (i.e., shallower than 1 km depth) where the dynamic displacements are the largest. This may be connected to the lasting of the passage of surface wave trains and linked to the use of Rayleigh waves with 20 s central period rather than 100 s. In fact, *Hill and Prejean* [2015] point out that the longer the period of the wave train, the longer the dynamic stress coherently imposed by the passing wave train lasts. Previous studies document dynamic triggering within hydrothermal systems caused by long-period surface waves [e.g., *Hill and Prejean*, 2015], but the underlying mechanisms remain poorly understood.

We propose that remote triggering by dynamic stresses of few kilopascals requires near-lithostatic fluid pore pressures at depth and the passing seismic waves simply advance the clock of a local seismic event that may have occurred anyway. As previously mentioned, the location uncertainty of the events triggered on 11 March 2011 at the LTGF does not allow us to speculate further about the physical state in the region of the triggered seismic events. Our results seem to indicate that dynamic triggering might be strongly controlled by the heterogenous distribution of pore pressures at depth.

#### Acknowledgments

This study has been carried out in the framework of an FNSNF Assistant Professor (AP) Energy Grant, (grant agreement PYAPP2\_166900). Raffaella De Matteis is thanked for providing the coordinates of the seismic stations used in *De Matteis et al.* [2008]. The catalog of earthquakes can be retrieved at <http://iside.rm.ingv.it/iside/standard/?lang=en> and the waveforms at <http://eida.gfz-potsdam.de/webdc3/>

#### References

- Aron, A., and J. L. Hardebeck (2009), Seismicity rate changes along the central California coast due to stress changes from the 2003  $M$  6.5 San Simeon and 2004  $M$  6.0 Parkfield earthquakes, *Bull. Seismol. Soc. Am.*, 99(4), 2280–2292, doi:10.1785/0120080239.
- Baldi, P., G. Bertini, A. Ceccarelli, and I. Dini (1995), Geothermal research in the Monteverdi Zone (western border of the Larderello geothermal field), paper presented at 1995 World Geothermal Congress, Florence, Italy.
- Bertini, G., M. Casini, G. Gianelli, and E. Pandeli (2006), Geological structure of a long-living geothermal system, Larderello, Italy, *Terra Nova*, 18(3), 163–169, doi:10.1111/j.1365-3121.2006.00676.x.
- Broggi, A. (2005), Contractional structures as relicts of the Northern Apennines collisional stage recorded in the Tuscan nappe of the Mt. Amiata geothermal area (Italy), *Boll. Soc. Geol. Ital., Volume speciale(4)*, 53–65.
- Broggi, A., A. Lazzarotto, D. Liotta, R. Nicolich, and G. Ranalli (2003), The  $k$ -horizon in the crust of the Larderello geothermal area (Southern Tuscany) | L'orizzonte  $K$  nella crosta dell'area geotermica di Larderello (Toscana meridionale), *Boll. Soc. Geol. Ital.*, 122(2), 103–116.
- Della Vedova, B., C. Vecellio, S. Bellani, and U. Tinivella (2008), Thermal modelling of the Larderello geothermal field (Tuscany, Italy), *Int. J. Earth Sci.*, 97(2), 317–332, doi:10.1007/s00531-007-0249-0.
- De Matteis, R., T. Vanorio, A. Zollo, S. Ciuffi, A. Fiordelisi, and E. Spinelli (2008), Three-dimensional tomography and rock properties of the Larderello-Travale geothermal area, Italy, *Phys. Earth Planet. Inter.*, 168(1–2), 37–48, doi:10.1016/j.pepi.2008.04.019.
- Dini, A., G. Gianelli, M. Puxeddu, and G. Ruggieri (2005), Origin and evolution of Pliocene-Pleistocene granites from the Larderello geothermal field (Tuscan Magmatic Province, Italy), *Lithos*, 81(1–4), 1–31, doi:10.1016/j.lithos.2004.09.002.

- Freed, A. M. (2005), Earthquake triggering by static, dynamic and postseismic stress transfer, *Annu. Rev. Earth Planet. Sci.*, 33(1), 335–367, doi:10.1146/annurev.earth.33.092203.122505.
- Fry, B., K. Chao, S. Bannister, Z. Peng, and L. Wallace (2011), Deep tremor in New Zealand triggered by the 2010  $M_w$  8.8 Chile earthquake, *Geophys. Res. Lett.*, 38, L15306, doi:10.1029/2011GL048319.
- Gomberg, J., P. A. Reasenberg, P. Bodin, and R. A. Harris (2001), Earthquake triggering by seismic waves following the Landers and Hector Mine earthquakes, *Nature*, 411(6836), 462–466, doi:10.1038/35078053.
- Gomberg, J., P. Bodin, K. Larson, and H. Dragert (2004), Earthquake nucleation by transient deformations caused by the  $M7.9$  Denali, Alaska, earthquake, *Nature*, 427(6975), 621–624.
- Gonzalez-Huizar, H., A. A. Velasco, Z. Peng, and R. R. Castro (2012), Remote triggered seismicity caused by the 2011,  $M9.0$  Tohoku-Oki, Japan earthquake, *Geophys. Res. Lett.*, 39, L10302, doi:10.1029/2012GL051015.
- Hill, D., and S. Prejean (2015), Dynamic triggering, in *Treatise on Geophysics*, 2nd ed., edited by G. Schubert, pp. 273–304, Elsevier, Amsterdam, doi:10.1016/B978-0-444-53802-4.00078-6.
- Hill, D., et al. (1993), Seismicity remotely triggered by the magnitude 7.3 Landers, California, earthquake, *Science*, 260(5114), 1617–1623.
- Hill, D. P. (2012), Surface-wave potential for triggering tectonic (nonvolcanic) tremor-corrected, *Bull. Seismol. Soc. Am.*, 102, 2337–2355, doi:10.1785/0120120086.
- Hill, D. P., F. Pollitz, and C. Newhall (2002), Earthquake volcano interactions, *Phys. Today*, 55(11), 41–47, doi:10.1063/1.1535006.
- Husen, S., R. Taylor, R. Smith, and H. Healer (2004), Changes in geyser eruption behavior and remotely triggered seismicity in Yellowstone National Park produced by the 2002  $M7.9$  Denali fault earthquake, Alaska, *Geology*, 32(6), 537–540, doi:10.1130/G20381.1.
- Hutton, L., and D. Boore (1987), *The  $M_L$  Scale in Southern California*, vol. 77, pp. 2074–2094.
- Jousset, P., and J. Rohmer (2012), Evidence for remotely triggered microearthquakes during salt cavern collapse, *Geophys. J. Int.*, 191(1), 207–223, doi:10.1111/j.1365-246X.2012.05598.x.
- Keller, J. V. A., and G. Piali (1990), Tectonics of the Island of Elba; A reappraisal, *Boll. Soc. Geol. Ital.*, 109(2), 413–425.
- Kiser, E., and M. Ishii (2011), The 2010  $M_w$  8.8 Chile earthquake: Triggering on multiple segments and frequency-dependent rupture behavior, *Geophys. Res. Lett.*, 38, L07301, doi:10.1029/2011GL047140.
- Kulhánek, O. (2002), *The Structure and Interpretation of Seismograms*, Academic Press, New York.
- Lienert, B. R., and J. Havskov (1995), A computer program for locating earthquakes both locally and globally, *Seismol. Res. Lett.*, 66(5), 26–36, doi:10.1785/gssrl.66.5.26.
- Lolli, B., P. Gasperini, and F. Mele (2015), Recalibration of the distance correction term for local magnitude ( $M_L$ ) computations in Italy, *Seismol. Res. Lett.*, 86, 1383–1391, doi:10.1785/0220150020.
- Lupi, M., E. H. Saenger, F. Fuchs, and S. A. Miller (2013), Lusi mud eruption triggered by geometric focusing of seismic waves, *Nat. Geosci.*, 6(8), 642–646, doi:10.1038/ngeo2239.
- Lupi, M., E. H. Saenger, F. Fuchs, and S. A. Miller (2014), Corrigendum: Lusi mud eruption triggered by geometric focusing of seismic waves, *Nat. Geosci.*, 7(8), 687–688, doi:10.1038/ngeo2239.
- Malinverno, A., and W. Ryan (1986), Extension in the Tyrrhenian Sea and shortening in the Apennines as result of arc migration driven by sinking of the lithosphere, *Tectonics*, 5, 7227–245.
- Manga, M., and E. Brodsky (2006), Seismic triggering of eruptions in the far field: Volcanoes and geysers, *Annu. Rev. Earth Planet. Sci.*, 34, 263–291.
- Matthews, M. V., and P. A. Reasenberg (1988), Statistical methods for investigating quiescence and other temporal seismicity patterns, *Pure Appl. Geophys.*, 126(2–4), 357–372, doi:10.1007/BF00879003.
- Mele, F., C. Marocci, and R. Moro (2007), ISIDE, Italian seismic instrumental and parametric data base. [Available at <http://iside.rm.ingv.it>]
- Miyazawa, M., and J. Mori (2006), Evidence suggesting fluid flow beneath Japan due to periodic seismic triggering from the 2004 Sumatra-Andaman earthquake, *Geophys. Res. Lett.*, 33, L05303, doi:10.1029/2005GL025087.
- Peng, Z., D. P. Hill, D. R. Shelly, and C. Aiken (2010), Remotely triggered microearthquakes and tremor in central California following the 2010  $M_w$  8.8 Chile earthquake, *Geophys. Res. Lett.*, 37, L24312, doi:10.1029/2010GL045462.
- Piccinini, D., N. A. Pino, and G. Saccorotti (2012), Emilia earthquakes Source complexity of the May 20, 2012  $M_w$  5.9, Ferrara (Italy) event, *Ann. Geophys.*, 55(4), 569–573, doi:10.4401/ag-6111.
- Pollitz, F., and R. Bürgmann (2014), The profound reach of the 11 April 2012  $M8.6$  Indian Ocean earthquake: Short term global triggering followed by a longer term global shadow, *Bull. Seismol. Soc. Am.*, 104, 972–984.
- Prejean, S. G. (2004), Remotely triggered seismicity on the United States West Coast following the  $M_w$  7.9 Denali Fault earthquake, *Bull. Seismol. Soc. Am.*, 94(6B), S348–S359, doi:10.1785/0120040610.
- Prejean, S. G. (2013), Where do we stand after twenty years of dynamic triggering studies, Abstract S43D-04 presented at 2013 Fall Meeting, AGU, San Francisco, Calif., 15–19 Dec.
- Ryder, I., A. Rietbrock, K. Kelson, R. Bürgmann, M. Floyd, A. Socquet, C. Vigny, and D. Carrizo (2012), Large extensional aftershocks in the continental forearc triggered by the 2010 Maule earthquake, Chile, *Geophys. J. Int.*, 188(3), 879–890, doi:10.1111/j.1365-246X.2011.05321.x.
- Saccorotti, G., D. Piccinini, F. Mazzarini, and M. Zupo (2013), Remotely triggered micro-earthquakes in the Larderello-Travale Geothermal Field (Italy) following the 2012 May 20,  $M_w$  5.9 Po-Plain earthquake, *Geophys. Res. Lett.*, 40, 835–840, doi:10.1002/grl.50254.
- Saccorotti, G., D. Piccinini, M. Zupo, F. Mazzarini, C. Chiarabba, N. P. Agostinetti, A. Licciardi, and M. Bagagli (2014), The deep structure of the Larderello-Travale Geothermal Field (Italy) from integrated, passive seismic investigations, *Energy Procedia*, 59, 227–234.
- Saenger, E. H., N. Gold, and S. A. Shapiro (2000), Modeling the propagation of elastic waves using a modified finite-difference grid, *Wave Motion*, 31(1), 77–92.
- Stacy, S. (2005), Introduction to special section: Stress transfer, earthquake triggering, and time-dependent seismic hazard, *J. Geophys. Res.*, 110, B05501, doi:10.1029/2005JB003692.
- Stein, R. S. (1999), The role of stress transfer in earthquake occurrence, *Nature*, 402(6762), 605–609, doi:10.1038/45144.
- Vanorio, T., R. De Matteis, A. Zollo, F. Batini, A. Fiordelisi, and B. Ciulli (2004), The deep structure of the Larderello-Travale geothermal field from 3D microearthquake traveltimes tomography, *Geophys. Res. Lett.*, 31, L07613, doi:10.1029/2004GL019432.
- Walter, T., and F. Amelung (2007), Volcanic eruptions following  $M9$  megathrust earthquakes: Implications for the Sumatra-Andaman volcanoes, *Geology*, 35(6), 539–542, doi:10.1130/G23429A.1.
- Zigone, D., et al. (2012), Triggering of tremors and slow slip event in Guerrero, Mexico, by the 2010  $M_w$  8.8 Maule, Chile, earthquake, *J. Geophys. Res.*, 117, B09304, doi:10.1029/2012JB009160.